A versatile ion beam spectrometer for studies of ion interaction with 2D materials

Schwestka, J.; Melinc, D.; Heller, R.; Niggas, A.; Leonhartsberger, L.; Winter, H.; Facsko, S.; Aumayr, F.; Wilhelm, R. A.;

Originally published:

August 2018

Review of Scientific Instruments 89(2018)8, 085101

DOI: https://doi.org/10.1063/1.5037798

Perma-Link to Publication Repository of HZDR:

https://www.hzdr.de/publications/Publ-27743

A versatile ion beam spectrometer for studies of ion interaction with 2D materials

Janine Schwestka,[1] David Melinc,[1] René Heller,[2] Anna Niggas,[1] Lukas Leonhartsberger,[1] Helmut Winter,[3] Stefan Facsko,[2] Friedrich Aumayr,[1] and Richard A. Wilhelm[1,2]

[1)] *TU Wien, Institute of Applied Physics, 1040 Vienna, Austria*[a)]

[2)] *Helmholtz-Zentrum Dresden-Rossendorf, Institute of Ion Beam Physics and Materials Research, 01328 Dresden, Germany*

[3)] *Humboldt Universität zu Berlin, Department of Physics, 12489 Berlin-Adlershof, Germany*

(Dated: 11 June 2018)

We present an ultra-high vacuum setup for ion spectroscopy of freestanding two-dimensional solid targets. An ion beam of different ion species (e.g. Xe with charge states from 1 to 44 and Ar with charge states from 1 to 18) and kinetic energies ranging from a few 10 eV to 400 keV is produced in an electron beam ion source. Ions are detected after their transmission through the 2D target with a position sensitive microchannel plate detector allowing the determination of the ions exit charge state as well as the scattering angle with a resolution of approx. 0.04°. Further, the spectrometer is mounted on a swiveling frame covering a scattering angle of ±8° with respect to the incoming beam direction. By utilizing a beam chopper we measure the time-of-flight of the projectiles and determine the energy loss when passing a 2D target with an energy uncertainty of about 2%. Additional detectors are mounted close to the target to observe emitted secondary particles and are read-out in coincidence with the position and time information of the ion detector. A signal in these detectors can also be used as a start trigger for time-of-flight measurements, which then yield an energy resolution of 1% and an approx. 1000-fold larger duty cycle. First results on the interaction of slow Xe^{30+} ions with a freestanding single layer of graphene obtained with the new setup are compared to recently published data where charge exchange and energy were measured by means of an electrostatic analyzer.

Keywords: slow highly charged ions, 2D materials, ion spectrometer, single layer graphene

I. INTRODUCTION

Recently, two-dimensional materials made their way into the spotlight of theoretical as well as experimental research. They offer a broad range of unique properties and novel phenomena not found in bulk materials. Especially their electronic and optical properties and the already discovered ways to modify them, make 2D materials to promising candidates for future electronic devices[1–5]. The thickness of only one or a few atomic layers of these materials demands high surface sensitivity of modification and analysis tools to tailor and control the properties of 2D materials[6,7]. Currently available ion beam setups (focused ion beams, MeV ion beams for elemental analysis, sputter guns, etc.) used for 10 nm to 1 μm thick layers typically lack this surface sensitivity due the relatively large penetration depth of the ions[8–12]. One way to increase surface sensitivity of ion beams is to reduce the kinetic energy. Low-energy ion scattering spectroscopy (LEIS), with ion energies in the range of 500 eV, is used for composition analysis of the target's surface. Another path to address the very first few atomic layers of a target, is the utilization of the potential energy stored especially in highly charged ions[14–22]. By increasing the ions charge state (i.e. increasing the internally stored energy) and reducing its velocity, large amount of energy can preferentially be deposited into the surface of a material and therefore also into a 2D target.

Analyzing the remaining charge state as well as the energy loss of the projectile after it passed the 2D layer may enable to adjust the tailoring process (i.e. energy deposition) for various 2D materials with different electronic and structural properties[23,24]. In addition, it gives insight in the neutralization process of highly charged ions (HCIs) interacting with matter and therefore aims for a comprehensive understanding of the involved charge transfer processes[25–33]. In this contribution, we report on a versatile setup for slow ion irradiation and spectroscopy of 2D materials. The design of the setup was driven by a fundamental research interest in ion-surface interaction and the need to improve our accessible electrostatic ion beam spectrometers with respect to the possibilities to observe arbitrarily large charge exchanges (i.e. also neutral particles) and boost data acquisition times by a factor of ∼100. The latter is especially important for 2D materials which degrade due to ion induced damage[18–20]. The kinetic and the potential energy of the projectile, which is deposited into the target and further dissipated into emission of secondary particles, is accessed by measuring the time-of-flight (TOF) of the ion[34–36] as well as its exit charge state, respectively. First proof-of-principle measurements for slow HCI transmission through a freestanding single layer of graphene (SLG) are presented. The obtained results are compared to studies on ion interaction with SLG performed with an electrostatic ana-

[a)] Author to whom correspondence should be addressed. Electronic mail: schwestka@iap.tuwien.ac.at

lyzer setup[37].

II. EXPERIMENTAL SETUP

An overview of the facility composed of an electron beam ion source (Dresden EBIS-A from Dreebit GmbH, Germany[38,39]) and our ion spectrometer with some basic dimensions is shown in Fig. 1. The ion beam is mass-to-charge separated by means of a Wien filter and guided via a self-designed electrostatic lens system into the target chamber. Close to the exit of the lens assembly, the beam is chopped by an electrostatic beam chopper providing an approx. 4 ns long ion pulse and the start signal for TOF measurements. The samples are mounted on a movable (x-,y-,z- and ϕ-axis) sample holder in the center of the setup. Its design enables transmission of the projectiles through the sample for rotation angles of up to 60° (self-shadowing for larger angles) and it holds up to three individual samples. Via a load-lock the holder can easily be transferred into the ultra-high vacuum chamber allowing fast sample exchange within 30 minutes. After the transmission through the sample, the projectiles enter the drift chamber. They pass a 0.5x10 mm horizontal slit and a pair of deflection plates. Depending on their charge state and kinetic energy they are deflected onto different positions of a microchannel plate detector (MCP). Equipped with a delay-line anode (delay-line detector (DLD), Roentdek GmbH, Germany), the MCP detector provides position information of the impinging projectiles with a resolution of about 100 μm. Due to the horizontally mounted deflection plates, the vertical position on the MCP yields the ion charge state and the horizontal position yields the scattering angle. Additionally, the MCP signal serves as the stop signal for the measured TOF of the ions. The pressure in the target chamber as well as in the drift chamber is kept below 1x10^{-8} mbar to prevent charge exchange with residual gas atoms. After bake-out a base pressure of below 1x10^{-9} mbar can be reached.

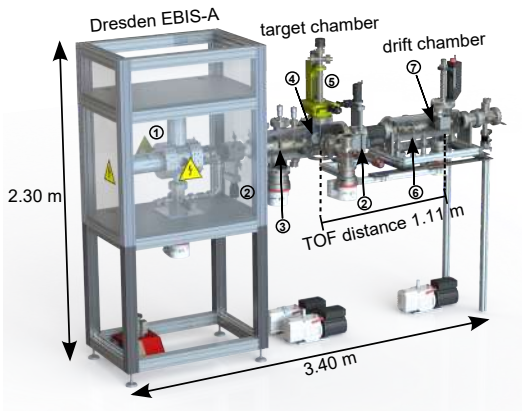

FIG. 1. (color online) Overview of the experimental setup. ① Electron beam ion source ② Pneumatic shutter ③ Electrostatic beam chopper ④ Electron emission statistics setup ⑤ Manipulator for x-,y-,z- and ϕ-rotation ⑥ Pair of deflection plates ⑦ MCP detector with delay-line anode.

A. Ion source and deceleration

Highly charged ions are produced in a room-temperature Dresden EBIS-A[38,39]. For Xenon as an operation gas, charge states of up to q=44 are available at electrical currents of >100 fA to several 10 pA with this type of ion source. The potential of the source is 9 kV determining an initial kinetic energy of q x 9 kV of the extracted ions. The base pressure in the source chamber is kept in the low 10^{-10} mbar range. Ions are confined in the source volume in axial direction by applying electric potentials to an arrangement of three drift tubes (Fig. 2) and in radial direction by the negative space charge of the electron beam, which is emitted from a cathode and triggers electron impact ionization in the source volume. Ions are extracted either in DC mode ('leaky mode') or 'pulsed mode', i.e. the potential of the last drift tube, U_b, on the extraction side is lowered in a way that only ions with sufficient thermal energy (E> q $\cdot$ ($U_b - U_a, U_a$: potential of middle drift tube, (Fig. 2)) are able to leave the trap continuously or this trap potential switches between two values creating 50 ns -100 μs ion pulses, respectively. The detailed working principle of these ion sources is described elsewhere[40]. The pulsed mode would in principle provide a pulsed beam to be used for our TOF measurements, but our power supplies used for U_b pulsing do not provide fast enough (<10 ns) voltage ramping. Since all ion charge states up to a maximum charge state (given by the electron beam energy $E_e = e(U_{cat} + U_0) \sim$12 keV) are extracted from the source volume, a Wien filter with an aperture of 1 mm is utilized to select a specific charge state for our experiments. After leaving the ensemble of drift tubes, for typical drift tube voltages, the kinetic energy of the emitted ions ranges from 9 keV up to 400 keV ($E_{kin} = U_b \cdot q$) depending on the charge state. In order to decelerate the ions, a negative potential U_{decel} can be applied to the ion source (incl. all power supplies galvanically isolated from ground through an isolating transformator) resulting in ions with in principle arbitrarily low kinetic energy. In praxis, a reasonable beam diameter at the sample of ~2 mm is only possible down to a few 10 eV x q ($E_{kin} = q \cdot (U_b - U_{decel})$). Reducing the initial kinetic energy of those ions leads to a radial spread of the resulting beam. A multi-segment system of electrostatic lenses for focusing of the beam was designed and simulated (using the SIMION code[41]) for this setup. With 7 individually biased segments we realize a stepwise deceleration and maintain therefore a reasonably good beam focus at a working distance of 460 mm. Two lens segments are split in horizontal and vertical direction enabling beam steering to correct for beam misalignment. The beam is further guided through the opening of the beam chopper and an arrangement of horizontal and vertical slit aper-

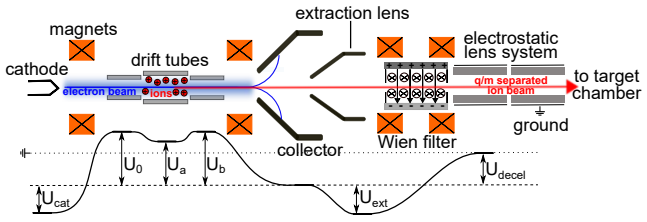

FIG. 2. (color online) Scheme of the ion extraction from an EBIS. HCIs ionized by an electron beam are trapped in an arrangement of drift tubes. The extracted beam is mass-to-charge separated in a Wien filter and further steered and focused with an electrostatic lens system. On the lower part the electrostatic potentials applied to each component are shown with respect to ground potential.

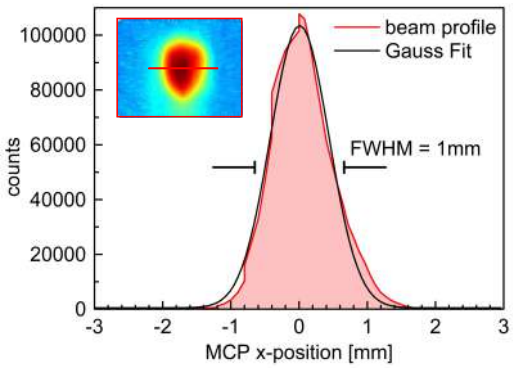

FIG. 3. (color online) DLD signal along the x-axis recorded for a 170 keV Xe^{30+} ion beam extracted from the EBIS-A and guided through the slit aperture system. The inset shows the 2D plot of the beam, the red line indicates the presented line profile.

tures. This allows selectable beam spot diameters of either 0.25 mm^2 or 1 mm^2 with a beam divergence of 0.04° or 0.09°, respectively. The spatial profile of the ion beam can be directly obtained from the DLD. The Gaussian shaped profile of a 170 keV Xe^{30+} ion beam, collimated in the target chamber by 0.5 mm slits in horizontal and vertical direction, is shown in Fig.3. The full width at half maximum (FWHM) of about 1 mm at the DLD and a spreading of the beam along the distance of 1105 mm between target and detector (allowed divergence of 0.04°), yields a beam spot diameter of 0.52 mm at the sample, which can be assumed well in agreement with the collimator openings. We want to emphasize here, that the presented ion spectrometer can be equipped with any kind of ion source (with a brightness of more than 10^{12} ions s^{-1} cm^{-2} sr^{-1} in order to achieve reasonable signal-to-noise ratio at the DLD), even though our research currently focuses on the interaction of HCIs with 2D materials.

B. Ion spectrometer

A schematic of the main part of the setup, the ion spectrometer, is shown in Fig.4. For precise TOF measurements and further energy loss calculations an appropriately short ion pulse is inevitable. The facility houses an electrostatic beam chopper with a spacing between the plates of 2 mm, a width of the deflection plates of 6 mm (perpendicular to the ion beam direction), and a plate length (in direction of the ion beam) of 2 mm, mounted 100 mm in front of the first slit aperture. The applied voltage to the chopper plates lifts the passing ion beam above the opening of the following slit aperture preventing the ions to reach the target. The required chopping voltage and the width of those pulses depend on the kinetic energy (or the ion charge state if a constant source potential is used) as well as on the ion mass. Ion pulses with pulse widths in the range of 4-10 ns for TOF measurements can be achieved (see Fig. 5).

Once the beam passed the chopper, ions hit the aperture (chopping voltage on) or pass another (biased) circular aperture and hit the target mounted on the sample holder (chopping voltage off). Due to the interaction process, particles can be sputtered and electrons as well as X-rays might be emitted depending on the sample and the ion species. The target chamber is equipped with an electron emission statistics (EES) setup perpendicular to the ion beam for measuring the number of these emitted low energy electrons[42–45]. The rotatable sample holder allows to turn the sample surface in order to reach high collection efficiencies for electrons (Cosine-emission profile[46]). Electrons emitted from the interaction process are collected through a grid (high transparency of about 95%) biased at +200 - +1000 V. Further, the circular aperture the ion beam has to pass on its way to the target is biased at -500 V. In this way electrons are efficiently collected by the grid and electrons created from ions impacting slit apertures (e.g. when the chopping voltage is on) are suppressed. After the grid, electrons are accelerated to 30 keV and are detected by a surface barrier detector. The electron flight time from the target surface to the detector amounts to approx. 2.5 ns and is only determined by the potentials applied, i.e. it is constant independent of the ions used[43]. Therefore, the timing signal from the surface barrier detector might provide an appropriate start signal for prospective TOF measurements enabling the use of a continuous ion beam and therefore increase the duty cycle of our spectrometer significantly. This is of particular importance when working with very high charge states where the available ion current is small (∼10 ions/s). Results for this mode of operation are shown below. Note, that especially for slow ions the applied potentials can lead to a deflection of the primary ion beam in front and after the transmission through the target. In this case, lower grid potentials as well as larger target-grid distances have to be chosen resulting in longer electron flight times (up to 20 ns for 10 eV electrons). Further, the vacuum chamber

houses enough space for possible mounting of additional detection systems, like a silicon drift detector for registering X-ray emission from samples irradiated with highly charged ions[29,47–49]. After the transmission through the target, the ions move field free into the drift chamber. The whole drift chamber is swiveling with an angle of $\phi \pm 8°$ with respect to the incident ion beam direction, which allows us to measure the scattering angle of transmitted projectiles up to relatively large angles. In order to perform charge state analysis, ions scattered in vertical direction are stopped by a horizontal slit aperture with an opening of 0.5x10 mm approx. 730 mm behind the target. The vertical angular acceptance of the drift chamber amounts therefore to 0.04°. Ions scattered in the horizontal plane can pass the slit up to an angle of ±0.25° with respect to the drift chamber axis (which can be swiveled). Depending on their charge state the ions are then further deflected in vertical direction in a set of deflection plates.

C. Charge exchange analysis

The charge states of ions after transmission through the target are analyzed by a 40 mm long pair of deflection plates with a gap of 21 mm between the plates (see Fig.4). At this point all ions have the same kinetic energy (neglecting the small amount of energy loss in the sample (few %)), but different charge states (due to charge exchange in the sample) in contrast to the case at the beam chopper (typically same E/q ratio). Each charge state experiences a different deflection resulting in a specific position at the following MCP detector (an additional, but comparatively small, vertical momentum component results from the vertical scattering angle acceptance (0.04°) of the drift chamber aperture as well as the kinetic energy distribution). The plates can be biased with voltages of up to 2 kV depending on the required charge state separation. The MCP detector is operated in a saturation mode at an amplification voltage of -1900 V applied to the front, guaranteeing the detection of different charged ions as well as neutral projectiles. To reduce the effect of post accelerating of the ions by the MCP front bias influencing the measured TOF, the entire MCP is housed in a grounded metal box with a highly transparent grid at the entrance. The MCP is further equipped with a delay-line anode (RoentDek DLD40 with an active area >40 mm) enabling two-dimensional position imaging of the received signal. The detectors position resolution of <0.1 mm[50] results in a scattering angle resolution of 0.01° (detector resolution without incident beam divergence). The position at the y-axis of the MCP defines the exit charge state q_{exit} according to

$$y = \frac{1}{2}\frac{U q_{exit}}{E_{kin}}\frac{l}{d}\left(\frac{l}{2} + s\right). \quad (1)$$

The y-position depends on the incident kinetic energy E_{kin} of the projectile, the applied deflection voltage U, the length of the deflection plates l, the gap between the plates d and the distance between the deflection plates and the MCP detector s. For a typical (initial) kinetic energy of Xe ions of 150 keV, a deflection voltage of 110 V is sufficient for a 1 mm separation of the charge states (necessary to prevent overlap from different charge states due to the vertical momentum component discussed above). However, if the initial charge state is >30 not all possible exit charge states can be measured in parallel (MCP diameter is limiting). Now, either the deflection voltage can be reduced leading to an overlap of charge states and subsequently to difficulties in data analysis or the DLD can be moved in vertical direction (mounted on a 150 mm travel linear feedthrough) and the charge state distribution is measured stepwise (typically 2 vertical positions of the DLD are enough). For even higher charge states q>50, the deflection plate separation must be increased mechanically (and the voltage increased) to prevent the highest charge states from hitting the plates themselves. The x-axis of the DLD represents the scattering angle of the projectiles within the horizontal plane. The aperture width of 10 mm (entrance of the drift chamber) limits the observable scattering angle to ±0.25°. The MCP diameter would cover an angular range of ±0.9°, however only at its center (y=0). Since the whole drift chamber including the MCP detector is swiveling, transmitted projectiles can be measured in an angular range of ±8° with an angular resolution of 0.04° (allowed divergence of ion beam) by subsequent measurements. Integrating the counts recorded at the MCP linewise over a certain scattering angle range (data projection on the y-axis) leads to a histogram of the exit charge state distribution after the transmission through the target (see Fig.7). Note, that the detection efficiency of the MCP shows a charge state dependency[51]. Nevertheless, for a reasonably biased MCP (>1800 V) the measured exit charge state intensities are not notably influenced by this varying efficiency.

D. Energy loss spectroscopy

After the interaction with a sample, the energy loss of the projectile can be calculated by measuring its time-of-flight. The ion beam with a specific incident charge state and kinetic energy is chopped by an electrostatic beam chopper. To create a suitable trigger signal for TOF measurements of keV to a few 100 keV ions a constant voltage is applied and further chopped with a frequency of a few hundred kHz by a fast pulsing electronics. It enables to switch off voltages of ±60 V applied to both deflection plates for 8-34 ns within a rise/fall time of 3-5 ns[52]. The electronics is triggered by a standard TTL pulse with a maximum frequency of 2 MHz. Fig. 5a shows an oscillograph of the voltages applied to both deflection plates for a typical setting of 34 ns opening time. This opening time needs to be adjusted to the ion velocity as indicated

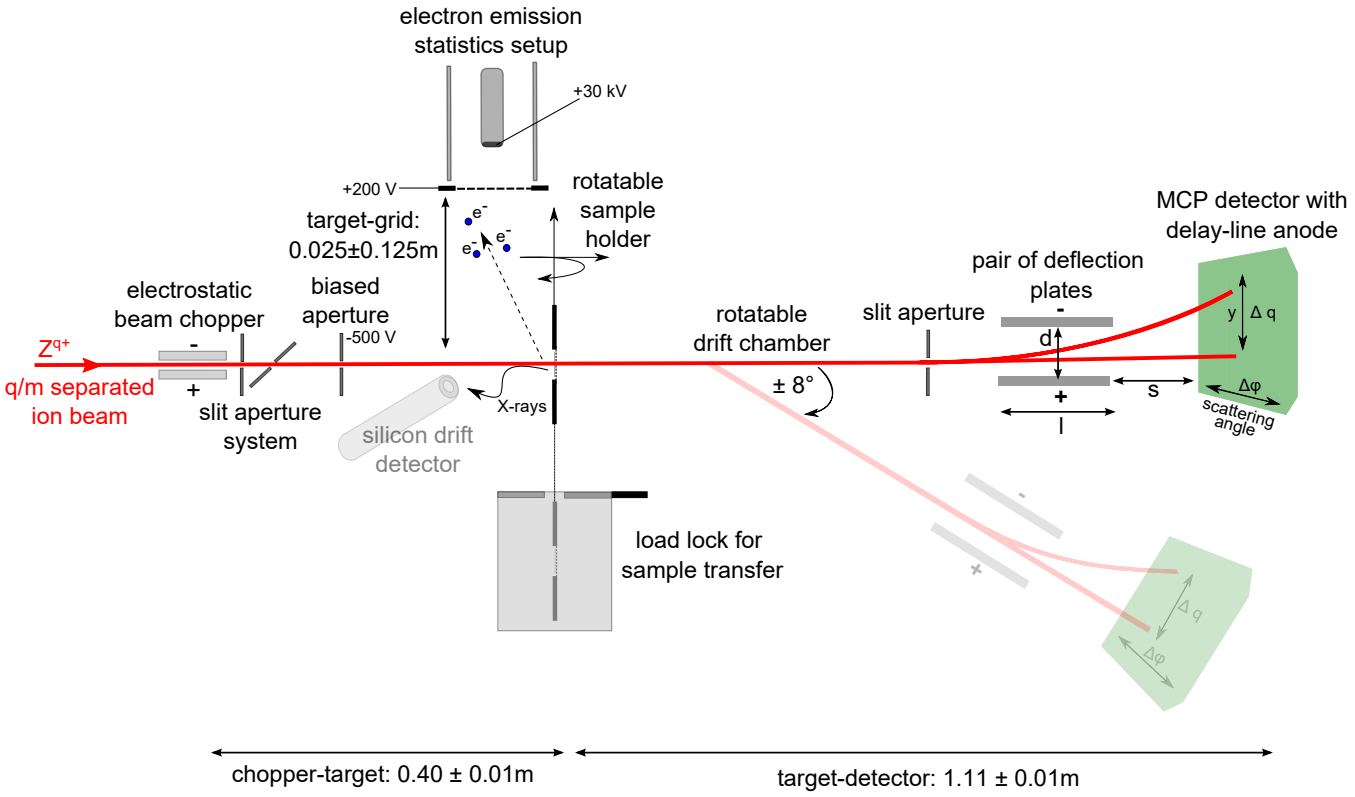

FIG. 4. (color online) Ion spectrometer for charge exchange and energy loss measurements of ions transmitted through free-standing 2D materials. The rotation of the drift chamber is out-of-plane to the sketch here.

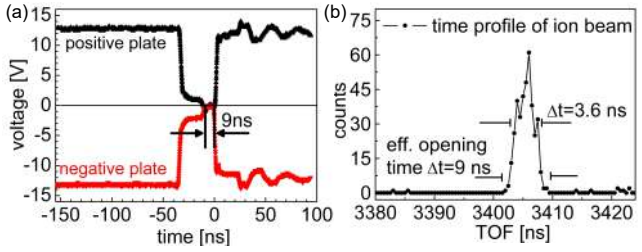

FIG. 5. (color online) (a) Voltage applied to electrostatic beam chopper. Even though the chopper opening time was set to the maximum (34 ns), a completely switching off (0 V) was only reached for a duration of 9 ns. (b) Measured TOF of 131 keV Xe^{30+} ions with an effective chopper opening time of 9 ns.

in Tab. 1, because a too short opening time will always blank the beam and a too long opening time blurs the TOF spectrum. Also, the necessary chopping voltage varies with ion velocity. A smaller voltage is advantageous since it reduces the overshooting effect after the steep fall/rise of the voltage (compare Fig. 5a). Nevertheless, the time the ions need to pass the chopper can exceed the adjustable opening time of 8-34 ns depending on their kinetic energy, limiting currently the lowest

TABLE I. Required chopping voltages and opening times of electrostatic beam chopper depending on the kinetic energy of the ion beam.

E_{kin}	Time ions pass chopper	Chopping voltage
3 keV	90 ns	± 0.3 V
30 keV	28 ns	± 3.2 V
100 keV	16 ns	± 10.7 V
150 keV	13 ns	± 16.2 V
300 keV	9 ns	± 32.4 V
350 keV	8 ns	± 37.8 V

possible kinetic energy for TOF measurements to about 30 keV for Xe ions. The MCP signal of the impinging ions delivers the required stop signal for the TOF measurements. The signal is taken from the MCP backside electrode (and not the delay-line anode), is pre-amplified, and a fast-NIM pulse is produced by a constant fraction discriminator. The TTL signal triggering the chopper is converted into a fast-NIM pulse as well and both timing signals are readout by a time-to-digital converter (Roentdek TDC8HP with a resolution of 55 ps). The time-of-flight of ions not passing a sample is used as reference to calculate the energy loss for projectiles interacting with a sample.

The timing resolution given by the constant fraction

discriminator used for the MCP signal can be neglected (<0.2 ns[50]). Therefore, the FWHM of the measured timing signal for a projectile without any energy straggling is found to be <4 ns, shown in Fig. 5b for 131 keV Xe^{30+} ions. The chopper plates have been set to a constant voltage of 26 V and with a frequency of 230 kHz the ion beam is chopped into ion pulses with a width of ∼9 ns. The maximum chopping frequency depends on the time the ions need to pass the chopper (depending on the ions initial energy). For 131keV Xe^{30+} ions frequencies above 10 MHz would easily be possible. Nevertheless, for frequencies >1/TOF several peaks in the TOF spectrum are received due to the long flight time of the ions from the chopper to the detector leading to an additional required data treatment. The initial energy distribution of ions emitted from the source might also contribute to the measured finite pulse width. This energy distribution is determined by the momentum distribution of the ions in the trap (heated by electron impact), small fluctuations of the U_0 and U_b potentials (<430 mV in leaky mode), and a variation of the initial ionization position in the source (different potential for the ions to start from with respect to the electron beam space charge distribution). Fluctuations of U_0 lead to an energy width of the extracted beam of 0.43 V x q. For ions starting from a source potential of 9 kV the subsequent broadening of the TOF signal can be neglected ($\Delta E_{fluc}/E<10^{-4}$), since the differences in the TOFs of these ions starting with slightly higher or lower energies are below the timing resolution. Therefore, we assume that the measured pulse width of ∼9 ns mainly results from the effective opening time of the chopper (chopping voltage switched off), in which the applied potential actually reaches 0 V at both blanking plates (also shown in Fig. 5a). The energy resolution ΔE of the spectrometer is directly proportional to the measured timing resolution Δt:

$$\frac{\Delta E}{E} = 2\frac{\Delta t}{t}. \qquad (2)$$

With a relative timing resolution of Δt/t ∼0.11% a relative energy resolution ΔE/E ∼0.21% for projectiles shown in Fig. 5b can be derived according to equation (2). The resolution is given by the FWHM in Fig. 5b and the precision is estimated by the value of the resolution (for very long measurements the precision would be much better). Nevertheless, the actual accuracy is ∼10 times below that resolution. Note, that we clearly distinguish between energy accuracy, precision and resolution[53]. The power supply used for the source potential U_0 has a voltage accuracy of ±82.75 V (standard values given by ISEG GmbH, Germany), which means in this case an offset in the actual applied voltage and not fluctuations in the potential. This accuracy leads to an energy uncertainty of ΔE∼2.5 keV (Xe^{30+}) of the extracted beam. For 131 keV Xe^{30+} ions, used in the presented TOF measurements, an energy accuracy of ΔE ∼2 x 10^{-2}E for calculating the energy loss can therefore be estimated. A high-precision

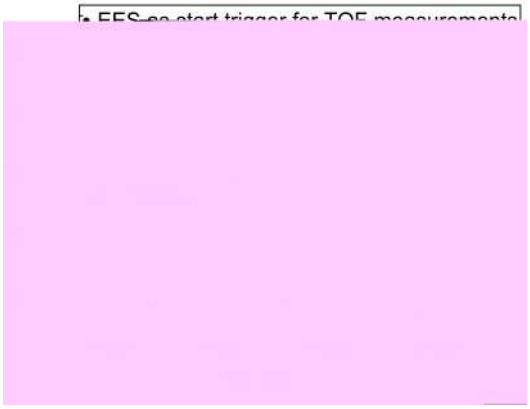

FIG. 6. TOF measured for 200 keV Xe^{23+} ions transmitted through SLG. Emitted electrons serve as a start trigger, ions impinging on the DLD deliver the required stop.

HV-voltmeter would help here in the future. Note, that the space charge potential of the electron beam will also contribute to the accuracy, but is not discussed here. As an additional approach, instead of chopping the ion beam with an electrostatic chopper, we can use ion induced electron emission from the sample as a trigger signal for TOF measurements. Within a delay of approx. 2.5 ns the electrons are registered at the surface barrier detector and again the DLD signal of the impinging ions serves as a stop trigger. Fig. 6 shows the measured TOF for 200 keV Xe^{23+} ions transmitted through SLG analyzed with a time-to-amplitude converter (ORTEC 566) and a multichannel analyzer (CAEN 8k N957). A relative timing resolution of Δt/t∼0.6% can be estimated from the FWHM of Δt=12.8 ns of the TOF peak in Fig. 6. Therefore, we find a relative energy resolution of ΔE/E∼1.2% for this operation mode. Note, that the data in Fig. 6 is taken for ions, which passed SLG and triggered electron emission, i.e. an energy straggling of the ions is present in contrast to the beam chopping method without target. Again, the precision can be estimated by the value of the resolution. Since we are not able to measure the TOF of the primary peak, which passes holes in the sample and therefore does not suffer energy loss or energy straggling in the sample (no electron emission), we are not able to calibrate our system as in the case of the electrostatic beam chopper method. Therefore, as long as an energy uncertainty of a few keV of the extracted ion beam remains, the accuracy for TOF measurements using EES as a trigger signal will be below the one found for chopping the ion beam (>2%). Nevertheless, this operation mode becomes favorable for very high charge states, where small ion currents (∼10 ions/s) require a continuous beam.

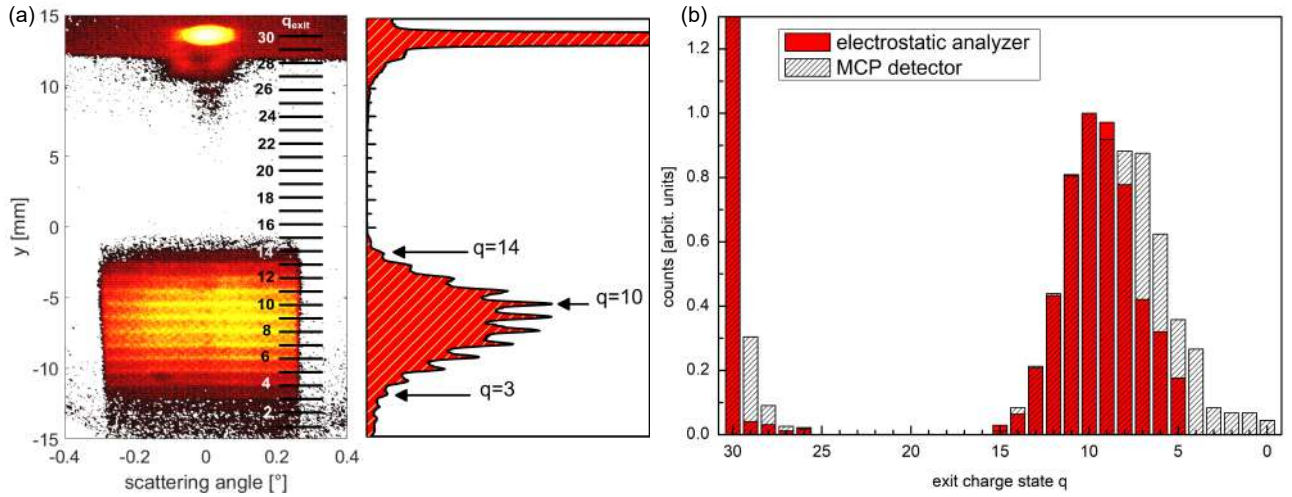

FIG. 7. (color online) (a) Exit charge state spectrum of 170 keV Xe^{30+} ions transmitted through SLG. Y-pos signal of MCP vs. scattering angle (left) and exit charge state spectrum vs. recorded counts (right) are shown. (b) Exit charge state distribution (a) integrated for a scattering angle range of ±0.25° and compared to data of ref. 37 recorded with an electrostatic analyzer (1.6° detection angle).

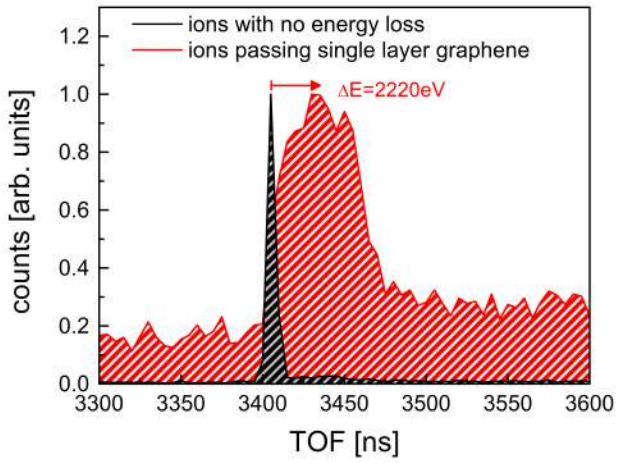

FIG. 8. (color online) Measured TOF for 131 keV Xe^{30+} ions transmitted through SLG.

III. RESULTS AND COMPARISON TO EXISTING DATA

The first ion spectroscopy studies with the new setup were performed on a freestanding monolayer graphene sheet. The thin film is suspended on a Quantifoil support on top of a transmission electron microscopy (TEM) grid, which delivers areas of freestanding SLG in the μm^2 range. The ions can easily pass those areas in the sample and further, with a thickness of only ∼0.3 nm, charge exchange and stopping of the transmitted ions can be directly measured. Recently, the interaction of slow HCI with SLG was investigated with an electrostatic analyzer[37]. We found a surprisingly effective charge exchange in this monolayer material. With the presented ion spectrometer setup we are able to verify those measurements and add data for larger charge exchanges not observable with an electrostatic analyzer, in particular for neutralized projectiles. The resulting exit charge state spectrum for 170 keV Xe^{30+} ions after transmission through a single layer of graphene is presented in Fig. 7. In comparison to the data acquired with the electrostatic analyzer the same mean exit charge state of q=10 is found, even though the spectrum shows a slightly broader distribution. We attribute this broadening to present contaminations on the sample during the measurement.

With the chopper based TOF approach described above the energy loss of 131 keV Xe^{30+} after the transmission through SLG was also measured. The recorded TOF for ions suffering no energy loss (q_{in}=q_{out}=30) is compared to the broad TOF peak for projectiles taking part in the charge exchange process and leading to the observed exit charge state distribution (TOF for all ions in charge states 2-15) can be seen in Fig. 8. The measured TOF is used to calculate the energy loss of the projectiles. The mean of the TOF peak for Xe^{2+}-Xe^{15+} ions yields an averaged energy loss of ΔE∼1.7% (2220 eV) for ions contributing to the exit charge state spectrum. Since we know from our previous measurements with an electrostatic analyzer, that the energy loss is closely connected to the charge exchange we can also determine the TOF for each impact position on the DLD from data stored in list-mode, i.e. for each scattering angle and charge exchange (not shown in this paper). With an energy accuracy of ΔE ∼2 x 10^{-2}E and averaged energy loss estimation for the whole exit charge state distribution, so far the TOF technique cannot compete with the high energy resolution of the electrostatic analyzer setup. Neverthe-

less the measured energy loss in SLG lies in the same order of magnitude as have been measured previously[54].

IV. CONCLUSION AND SUMMARY

We present a new setup for ion spectroscopy on two-dimensional materials. Charge exchange can be studied as well as energy loss of the projectile by measuring its TOF. First results are compared to transmission studies performed with an electrostatic analyzer setup. The recorded exit charge state spectrum is well in agreement with earlier studies and allows access to low charged and already neutralized particles in addition. This might become crucial for continuative studies on other 2D materials, where the whole exit charge state distribution might be shifted to lower exit charge states depending on the material properties. Further, measuring the spectrum with a position sensitive MCP detector yields in the recording of exit charge states depending on their scattering angle with a high resolution of $<0.05°$. By recording all charge states at the same time, we can increase data acquisition rates by a factor of $\sim$100 compared to measurement with an electrostatic analyzer, where charge states are recorded sequentially. This will again be advantageous for ion transmission studies on 2D materials, which suffer severe irradiation damage. So far, from our TOF measurements we get an estimation for the energy loss in SLG averaged over all projectiles taking part in the charge exchange process. Nevertheless, ten times higher energy resolution is found when measuring the projectiles energy loss with an electrostatic analyzer. In the future the detection of emitted electrons and/or X-rays in coincidence with transmitted projectiles allows access to further details of the interaction process. When exchanging highly charged particles to projectiles like H, D or He, the ion spectrometer might also enable grazing incidence fast atom diffraction (GIFAD) spectroscopy on 2D materials. Therefore, simply the scattering angle limiting aperture at the entrance of the drift chamber has to be removed and two-dimensional momentum information on the scattered projectiles can be accessed.

ACKNOWLEDGMENTS

The authors want to thank for the financial support from the doctoral college program TU-D funded by the TU Wien. Further, Marika Schleberger and Roland Kozubek are gratefully acknowledged for support with suitable freestanding samples. We express our gratitude to the Ion Beam Center of the Helmholtz-Zentrum Dresden-Rossendorf, where measurements with the electrostatic analyzer setup were performed and for lending the EBIS-A used in this study.

[1] H. Li, Z. Yin, Q. He, H. Li, X. Huang, G. Lu, D. W. H. Fam, A. I. Y. Tok, Q. Zhang, and H. Zhang, Small **8**, 63 (2012).
[2] M. M. Furchi, D. K. Polyushkin, A. Pospischil, and T. Mueller, Nano Letters (2014).
[3] A. Pospischil and T. Mueller, Applied Sciences **6**, 78 (2016).
[4] S. Schuler, D. Schall, D. Neumaier, L. Dobusch, O. Bethge, B. Schwarz, M. Krall, and T. Mueller, Nano Letters **16**, 7107 (2016).
[5] S. Wachter, D. K. Polyushkin, O. Bethge, and T. Mueller, Nature Communications **8**, 14948 (2017).
[6] O. Ochedowski, B. K. Bussmann, B. B. Etat, H. Lebius, M. Schleberger, B. B. D'Etat, H. Lebius, and M. Schleberger, Applied Physics Letters **102**, 153103 (2013).
[7] L. Madauß, O. Ochedowski, H. Lebius, B. Ban-d'Etat, C. H. Naylor, C. A. T. Johnson, J. Kotakoski, and M. Schleberger, 2D Materials **4**, 015034 (2017).
[8] K. Y. Ahn, M. Wittmer, and C. Y. Ting, Thin Solid Films **107**, 45 (1983).
[9] J. Ghatak, B. Satpati, M. Umananda, P. V. Satyam, K. Akimoto, K. Ito, and T. Emoto, Nuclear Instruments and Methods in Physics Research Section B: Beam Interactions with Materials and Atoms **244**, 64 (2006).
[10] E. Akcöltekin, S. Akcöltekin, O. Osmani, A. Duvenbeck, H. Lebius, and M. Schleberger, New Journal of Physics **10**, 53007 (2008).
[11] M. Döbeli, Journal of Physics: Condensed Matter **20**, 264010 (2008).
[12] R. Wirth, Chemical Geology **261**, 217 (2009).
[13] J. H. Freeman, W. Temple, D. Beanland, and G. A. Gard, Nuclear Instruments and Methods **135**, 1 (1976).
[14] G. Hayderer, S Cernusca, M Schmid, P Varga, H P Winter, F Aumayr, Physica Scripta **2001**, 156 (2001).
[15] M. Tona, H. Watanabe, S. Takahashi, Y. Fujita, T. Abe, S. Jian, N. Nakamura, N. Yoshiyasu, C. Yamada, M. Sakurai, and S. Ohtani, Journal of Physics: Conference Series **58**, 331 (2007).
[16] F. Aumayr, A. S. El-Said, and W. Meissl, Nuclear Instruments and Methods in Physics Research Section B: Beam Interactions with Materials and Atoms **266**, 2729 (2008).
[17] F. Aumayr, S. Facsko, A. S. El-Said, C. Trautmann, and M. Schleberger, Journal of Physics: Condensed Matter **23**, 393001 (2011).
[18] J. Hopster, R. Kozubek, J. Krämer, V. Sokolovsky, and M. Schleberger, Nuclear Inst. and Methods in Physics Research, B **317**, 165 (2013).
[19] J. Hopster, R. Kozubek, B. Ban-d'Etat, S. Guillous, H. Lebius, and M. Schleberger, 2D Materials **1**, 011011 (2014).
[20] R. A. Wilhelm, A. S. El-said, F. Krok, R. Heller, E. Gruber, F. Aumayr, and S. Facsko, Progress in Surface Science **90**, 377 (2015).
[21] A. S. El-Said, R. A. Wilhelm, R. Heller, M. Sorokin, S. Facsko, and F. Aumayr, Phys. Rev. Lett. **117**, 126101 (2016).
[22] P. Ernst, R. Kozubek, L. Madauß, J. Sonntag, A. Lorke, and M. Schleberger, Nuclear Inst. and Methods in Physics Research, B **382**, 71 (2016).
[23] O. Ochedowski, K. Marinov, N. Scheuschner, A. Poloczek, B. K. Bussmann, J. Maultzsch, and M. Schleberger, Beilstein Journal of Nanotechnology **5**, 291 (2014).
[24] Z. Li and F. Chen, Applied Physics Reviews **4**, 11103 (2017).
[25] M. Barat and P. Roncin, Journal of Physics B: Atomic, Molecular and Optical Physics **25**, 2205 (1992).
[26] R. Herrmann, C. L. Cocke, J. Ullrich, S. Hagmann, M. Stoeckli, and H. Schmidt-Boecking, Phys. Rev. A **50**, 1435 (1994).
[27] V. A. Morosov, A. Kalinin, Z. Szilagyi, M. Barat, and P. Roncin, Review of Scientific Instruments **67**, 2163 (1996).
[28] A. Arnau, F. Aumayr, P. M. Echenique, M. Grether, W. Heiland, J. Limburg, R. Morgenstern, P. Roncin, S. Schippers, R. Schuch, N. Stolterfohff, P. Varga, T. J. M. Zouros, H. P. Winter, D. F. D. Materiales, and P. Vasco, Surface Science Reports **27**, 113 (1997).
[29] T. Schenkel, A. V. Hamza, A. V. Barnes, and D. H. Schneider, Progress in Surface Science **61**, 23 (1999).

[30]S. Martin, R. Brédy, J. Bernard, J. Désesquelles, and L. Chen, Phys. Rev. Lett. **89**, 183401 (2002).
[31]T. Jahnke, A. Czasch, M. S. Schöffler, S. Schössler, A. Knapp, M. Käsz, J. Titze, C. Wimmer, K. Kreidi, R. E. Grisenti, A. Staudte, O. Jagutzki, U. Hergenhahn, H. Schmidt-Böcking, and R. Dörner, Physical Review Letters **93**, 163401 (2004).
[32]T. Jahnke, Journal of Physics B: Atomic, Molecular and Optical Physics **48**, 82001 (2015).
[33]R. A. Wilhelm, E. Gruber, J. Schwestka, R. Kozubek, T. T. I. Madeira, J. J. P. Marques, J. Kobus, A. V. A. Krasheninnikov, M. Schleberger, and F. Aumayr, Physical Review Letters **119**, 103401 (2017).
[34]S. N. Markin, D. Primetzhofer, M. Spitz, and P. Bauer, Phys. Rev. B **80**, 205105 (2009).
[35]M. K. Linnarsson, A. Hallén, J. Åström, D. Primetzhofer, S. Legendre, and G. Possnert, Review of Scientific Instruments **83**, 95107 (2012).
[36]S. Lohmann and D. Primetzhofer, Nuclear Instruments and Methods in Physics Research Section B: Beam Interactions with Materials and Atoms **423**, 22 (2018).
[37]E. Gruber, R. A. Wilhelm, R. Petuya, V. Smejkal, R. Kozubek, A. Hierzenberger, B. C. Bayer, I. Aldazabal, A. K. Kazansky, F. Libisch, A. V. Krasheninnikov, M. Schleberger, S. Facsko, A. G. Borisov, A. Arnau, and F. Aumayr, Nature Communications **7**, 13948 (2016).
[38]G. Zschornack, M. Kreller, V. P. Ovsyannikov, F. Grossman, U. Kentsch, M. Schmidt, F. Ullmann, and R. Heller, Review of Scientific Instruments **79**, 02A703 (2008).
[39]M. Schmidt, H. Peng, G. Zschornack, and S. Sykora, Review of Scientific Instruments **80**, 63301 (2009).
[40]E. D. Donets and V. P. Ovsyannikov, Sov. Phys. JETP **53(3)**, 466 (1981).
[41]D. A. Dahl, International Journal of Mass Spectrometry **200**, 3 (2000).
[42]G. Lakits, F. Aumayr, and H. Winter, Review of Scientific Instruments **60**, 3151 (1989).
[43]F. Aumayr, G. Lakits, and H. Winter, Applied Surface Science **47**, 139 (1991).
[44]H. Kurz, F. Aumayr, H. P. Winter, D. Schneider, M. A. Briere, and J. W. McDonald, Physical Review A **49**, 4693 (1994).
[45]H. Winter and H. P. Winter, EPL (Europhysics Letters) **62**, 739 (2003).
[46]D. Hasselkamp, H. Rothard, K.-O. Groeneveld, J. Kemmel, P. Varga, and H. Winter, in *Part. Induc. Electron Emiss. II, Vol. 123 of Springer Tracts in Modern Physics, Springer-Verlag, Berlin/Heidelberg* (1992).
[47]J. P. Briand and M. Benhachoum, Nuclear Inst. and Methods in Physics Research, B **267**, 665 (2009).
[48]M. Trassinelli, C. Prigent, E. Lamour, F. Mezdari, J. Mérot, R. Reuschl, J.-P. Rozet, S. Steydli, and D. Vernhet, Journal of Physics B: Atomic, Molecular and Optical Physics **45**, 85202 (2012).
[49]J. Schwestka, R. A. Wilhelm, E. Gruber, R. Heller, R. Kozubek, M. Schleberger, S. Facsko, and F. Aumayr, Nuclear Instruments and Methods in Physics Research, Section B: Beam Interactions with Materials and Atoms **422** (2018).
[50]RoentDek Handels GmbH, *http://www.roentdek.com/* ([Online, accessed 18-Jan-2018]).
[51]R. A. Wilhelm, *Wechselwirkung langsamer hochgeladener Ionen mit Ionenkristalloberflächen und ultradünnen Kohlenstoffmembrane*, Ph.D. thesis, Ph.D. Thesis Technische Universität Dresden (2014).
[52]N. Klingner, R. Heller, G. Hlawacek, J. V. Borany, J. Notte, J. Huang, and S. Facsko, Ultramicroscopy **162**, 91 (2016).
[53]"Iso 5725-1: Accuracy (trueness and precision) of measurement method and results - part i: General principles and definitions," (1994).
[54]E. Gruber, *Interaction of ions with 2D and 3D materials*, Ph.D. thesis, Ph.D. Thesis TU Wien (2017).